# Second-Order Perturbation Theory with Spin-Symmetry-Projected Hartree−Fock

Takashi Tsuchimochi*,[†] and Seiichiro L. Ten-no[†,‡]

[†]Graduate School of System Informatics and [‡]Graduate School of Science, Technology, and Innovation, Kobe University, 1-1 Rokkodai-cho, Nada-ku, Kobe 657-8501, Japan

ABSTRACT: We propose two different schemes for second-order perturbation theory with spin-projected Hartree−Fock. Both schemes employ the same *ansatz* for the first-order wave function, which is a linear combination of spin-projected configurations. The first scheme is based on the normal-ordered projected Hamiltonian, which is partitioned into the Fock-like component and the remaining two-particle-like contribution. In the second scheme, the generalized Fock operator is used to construct a spin-free zeroth-order Hamiltonian. To avoid the intruder state problem, we adopt the level-shift techniques frequently used in other multireference perturbation theories. We describe both real and imaginary shift schemes and compare their performances on small systems. Our results clearly demonstrate the superiority of the second perturbation scheme with an imaginary shift over other proposed approaches in various aspects, giving accurate potential energy curves, spectroscopic constants, and singlet−triplet splitting energies. We also apply these methods to the calculation of spin gaps of transition-metal complexes as well as the potential energy curve of the chromium dimer.
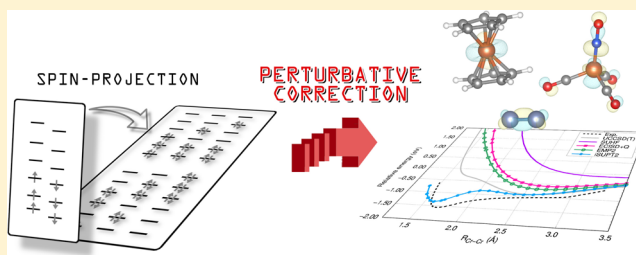
1. INTRODUCTION

In electronic structure theory, the Schrödinger equation is almost always unsolvable because of the exponential growth of the Hilbert space with system size; therefore, the equation is frequently approximated by a computationally solvable model. Such an approach has turned out to be fairly effective for computing many chemically important properties if the model used is well suited to the problem. In most cases, a single determinantal wave function of Hartree−Fock (HF) represents a qualitatively correct wave function at zeroth order and is employed as a starting point to add the remaining *dynamical correlation* effects by accounting for a large number of single- and double-electron substitutions (SD), each with a small contribution. There are many such single-reference (SR) methods, including Møller−Plesset perturbation theory (MP),[1] configuration interaction (CI), and coupled cluster (CC).[2,3] However, there are certain systems where multiple determinants have significant weights in the exact wave function. As a result, HF can introduce tremendous error by neglecting *static correlation*, which is a different type of electron correlation than dynamical correlation. To capture static correlation, one has to consider a multiconfiguration (MC) wave function, and significant effort has been made to develop multireference (MR) methods that can treat both dynamical and static correlation effects simultaneously.

The recent advancements and developments in MR methods have been largely based on the complete-active-space self-consistent field (CASSCF). Arguably, one of the most prominent approaches is CASPT2 (i.e., second-order perturbation theory (PT2) with a CASSCF wave function).[4,5] CASPT2 has been applied extensively to various applications because of its relatively low computational cost compared to that of MRCI[6,7] and MRCC.[8,9] Still, CASPT2 requires the construction of a CASSCF wave function and the diagonalization of a three-particle reduced density matrix (3RDM) within the active space, both of which can often become computational bottlenecks with a large active space.[10]

There are other paths to obtaining MC wave functions, and one possibility is symmetry-projected HF (PHF).[11] It has been well known for a relatively long time that a broken-symmetry determinant $|\Phi_0\rangle$ effectively contains multiple determinants as a mixture of states with different symmetries. Among several symmetries, spin symmetry is considered to be the most essential symmetry that HF violates in order to introduce a static correlation. Hence, applying a spin-projection operator $\hat{P}$ to unrestricted HF (UHF) makes it possible to generate a compact MC wave function $\hat{P}|\Phi_0\rangle$. In practice, molecular orbitals in $|\Phi_0\rangle$ are relaxed self-consistently in the presence of $\hat{P}$ by minimizing its energy, and as a result, $\hat{P}|\Phi_0\rangle$ can be regarded as a relatively efficient and reasonable MCSCF wave function. This method is referred to as spin-projected UHF (SUHF) and is expected to offer a suitable platform for subsequent dynamical correlation treatment.

It should be noted that the concept of spin projection emerged in the seminal work of Löwdin in the mid-1950s.[12] However, the difficulty of handling the many-body nature of a spin-projection operator has long hindered the development of its extension to treating dynamical correlation.[13,14] The first post-PHF method was proposed by Schlegel in 1986,[15,16]

followed shortly after by Knowles and Handy,[17,18] where spin-unrestricted MP2 (UMP2) was approximately spin-projected. Only recently has spin-extended MP2 (EMP2) been introduced, which performs numerically *exact* spin projection onto an MP1 wave function constructed from the underlying broken-symmetry determinant $|\Phi_0\rangle$ of SUHF (rather than UHF).[19] Since then, various post-SUHF methods have been developed, including time-dependent SUHF,[20] CI,[21,22] and CC.[23−28] These methods have been shown to generally outperform their restricted and unrestricted variants, especially when static correlation plays a key role. However, in the course of numerous test applications of the developed methods, we have found that the improvements the original EMP2 has to offer are somewhat limited, given the considerable improvements of spin-projected CI over unrestricted CI.[21,22] For instance, while the original EMP2 works well for biradicals, such as single-bond dissociation, its accuracy becomes substantially worse for more complicated cases, such as double and triple bond breaking, as will be discussed below. Furthermore, the predetermined nature of the first-order wave function does not allow the corresponding Hylleraas functional to be defined,[29,30] which would be useful in developing the geometry optimization method.[31,32] Given that perturbation theory is not unique and its performance is greatly dependent on the choice of the zeroth-order Hamiltonian, we believe it is desirable to continue exploring the possibility of more appropriate perturbation schemes for SUHF.

To this end, in this article we propose and test two perturbative corrections on SUHF. The first one is regarded as a generalization of the original EMP2 of Tsuchimochi and Van Voorhis,[19] which will be referred to as EMP2(0) hereafter to distinguish it from the newly developed EMP2 in the present work. It is based on the normal-ordered Hamiltonian introduced for the nonorthogonal determinants that appear in the integration of spin projection.[24] In the second scheme, which we call SUPT2, the so-called generalized Fock matrix is used as a starting point, as in CASPT2.[4,5] Consequently, SUPT2 shares many common properties as well as limitations with CASPT2. Indeed, it will be demonstrated below that the notorious intruder state problem is also inevitable in SUPT2, and we therefore also develop the level-shift technique frequently used in CASPT2.[33−35] In this work, their performances are compared by using simple test systems as well as transition-metal complexes.

This article is organized as follows. Section 2.1 presents an overview of SUHF. In Section 2.2, we apply the Rayleigh−Schrödinger perturbation theory with an SUHF reference and consider two possible *ansätze* for the first-order wave function. Section 2.3 reviews EMP2(0) and proposes the generalized EMP2, and Section 2.4 describes the SUPT2 theory. We introduce real and imaginary level shifts in Section 2.5, the latter of which requires some elaboration. Section 4 first presents a comparison among several methods tested for the HF, H_2O, and N_2 molecules and discusses the intruder state problem in SUPT2. It also presents the results for the spectroscopic constants of N_2, singlet−triplet splitting energies of various systems including transition metal complexes, and the potential energy curve of the Cr_2 molecule. In Section 5, we discuss the main cause of the different behaviors between EMP2 and SUPT2. Finally, conclusions are drawn in Section 6.

2. THEORY

2.1. Spin-Projected Unrestricted Hartree−Fock. Here, we briefly review SUHF and define some quantities that will be required in the following sections. Below, i, j, k, and l will represent occupied spin orbitals in $|\Phi_0\rangle$, and a, b, c, and d will represent virtual spin orbitals. General spin orbitals are denoted by p, q, r, and s. Because our approach is based on spin-unrestricted orbitals, in some cases, we will use $\sigma = \alpha,\beta$ to specify the spin of orbitals. Capital letters are used for spin-restricted orbitals.

In this work, a spin-projection operator $\hat{P}$ is given by the following form

$$\hat{P} = \frac{2S + 1}{8\pi^2} \int_\Omega d\Omega \, w(\Omega) \, \hat{R}(\Omega) \tag{1}$$

where $\Omega = (\alpha, \beta, \gamma)$ are the Euler angles, $w(\alpha, \beta, \gamma)$ are Wigner's D-matrix elements representing *fixed* weights, and

$$\hat{R}(\alpha, \beta, \gamma) = e^{-i\alpha\hat{S}_z}e^{-i\beta\hat{S}_y}e^{-i\gamma\hat{S}_z} \tag{2}$$

are the spin-rotation operators. Accordingly, $\hat{R}(\Omega)|\Phi_0\rangle$ gives a different determinant that is not orthogonal to $|\Phi_0\rangle$. Discretizing $\hat{P}$ with N_g grid points labeled by g, we write an SUHF wave function as

$$\hat{P}|\Phi_0\rangle = \sum_g^{N_g} w_g\hat{R}_g|\Phi_0\rangle \tag{3}$$

which is regarded as a linear combination of nonorthogonal determinants. Because $\hat{P}$ is idempotent, Hermitian, and commutable with the nonrelativistic Hamiltonian $\hat{H}$, the SUHF energy is simply given by

$$E_{\text{SUHF}} = \frac{\langle\Phi_0|\hat{H}\hat{P}|\Phi_0\rangle}{\langle\Phi_0|\hat{P}|\Phi_0\rangle} \tag{4}$$

The variational principle applied to SUHF gives the generalized Brillouin theorem

$$\langle\Phi_0|\hat{a}_a^i(\hat{H} - E_{\text{SUHF}})\hat{P}|\Phi_0\rangle = 0 \tag{5}$$

where $\hat{a}_q^p$ represents a single excitation operator from the qth to pth orbital.

It will prove useful later to introduce the normal-ordered products $\{\cdots\}_g$ for two nonorthogonal determinants $|\Phi_0\rangle$ and $\hat{R}_g|\Phi_0\rangle$,[21,22] meaning

$$\langle\Phi_0|\{\cdots\}_g\hat{R}_g|\Phi_0\rangle \equiv 0 \tag{6}$$

Using this definition, it is easy to show that the second-quantized Hamiltonian $\hat{H}$ can be written as[24]

$$\hat{H} = \sum_{pq} h_{pq}\hat{a}_q^p + \frac{1}{4} \sum_{pqrs} \langle pq\|rs\rangle\hat{a}_{rs}^{pq} \tag{7}$$

$$= E_g + \sum_{pq} (\mathbf{F}_g)_{pq} \{\hat{a}_q^p\}_g + \frac{1}{4} \sum_{pqrs} \langle pq\|rs\rangle\{\hat{a}_{rs}^{pq}\}_g \tag{8}$$

for *any* g, where $\langle pq\|rs\rangle$ are the standard antisymmetrized two-electron integrals and

$$E_g = \frac{\langle\Phi_0|\hat{H}\hat{R}_g|\Phi_0\rangle}{\langle\Phi_0|\hat{R}_g|\Phi_0\rangle} \tag{9}$$

$$(\mathbf{F}_g)_{pq} = h_{pq} + \sum_{rs} \langle pr \| qs \rangle \frac{\langle \Phi_0 | \hat{a}_s^r \hat{R}_g | \Phi_0 \rangle}{\langle \Phi_0 | \hat{R}_g | \Phi_0 \rangle} \tag{10}$$

are the transition energy and transition Fock matrix, respectively. The required matrix elements in this work can be easily derived using the Wick theorem extended to the nonorthogonal representation.[21] For further details, the reader can refer to refs [11], [21], and [22].

2.2. Perturbation Theory. In the Rayleigh–Schrödinger perturbation theory, the Hamiltonian is partitioned as

$$\hat{H} = \hat{H}_0 + \lambda \hat{V} \tag{11}$$

and the exact FCI wave function and its energy are expanded as

$$|\Psi\rangle = |\psi_0\rangle + \lambda |\psi_1\rangle + \lambda^2 |\psi_2\rangle + \cdots \tag{12}$$

$$E = E_0 + \lambda E_1 + \lambda^2 E_2 + \cdots \tag{13}$$

The choice of $\hat{H}_0$ is left arbitrary and will thus be determined later. As is well known, the order-by-order expansion of the Schrödinger equation results in

$$\hat{H}_0 |\psi_0\rangle = E_0 |\psi_0\rangle \tag{14}$$

and

$$(\hat{H}_0 - E_0)|\psi_n\rangle + \hat{V}|\psi_{n-1}\rangle = E_n |\psi_0\rangle + \sum_{k=1}^{n-1} E_{n-k} |\psi_k\rangle \tag{15}$$

In this work, we wish to formulate a perturbation theory using an SUHF wave function as the reference zeroth-order wave function:

$$|\psi_0\rangle \equiv \hat{P} |\Phi_0\rangle \tag{16}$$

To do so, first we have to develop an *ansatz* for $|\psi_1\rangle$ for the second-order energy E_2. Generally, higher-order wave functions have to be cleanly separated from the reference state. This means that they are orthogonal to each other:

$$\langle \psi_0 | \psi_1 \rangle = 0 \tag{17}$$

This can be accomplished by defining the projection operator that projects onto the reference space

$$\hat{\mathcal{P}}_0 \equiv \frac{|\psi_0\rangle\langle\psi_0|}{\langle\psi_0|\psi_0\rangle} = \frac{\hat{P}|\Phi_0\rangle\langle\Phi_0|\hat{P}}{\langle\Phi_0|\hat{P}|\Phi_0\rangle} \tag{18}$$

and its complementary projector

$$\hat{Q}_0 = 1 - \hat{\mathcal{P}}_0 \tag{19}$$

Using $\hat{Q}_0$, $|\psi_1\rangle$ can be generally expanded as

$$|\psi_1\rangle = \sum_{\Omega} \hat{Q}_0 |\Omega\rangle t_\Omega \tag{20}$$

where the basis $\{|\Omega\rangle\}$ spans the first-order interacting space of $|\psi_0\rangle$ and t_Ω represents the amplitude coefficients. The form of $\{|\Omega\rangle\}$ needs to be determined.

As in standard MRPT2 schemes, a natural choice for $\{|\Omega\rangle\}$ would be internally contracted configurations with respect to an SUHF wave function. In this case, only the singles and doubles spaces are needed, although the former does not

contribute to the second-order energy if the Brillouin theorem is satisfied. Therefore, the unitary-group-generator $\hat{\mathcal{E}}_\Omega$ may be used to produce such a basis

$$|\Omega\rangle = \hat{\mathcal{E}}_\Omega \hat{P} |\Phi_0\rangle \tag{21}$$

Viewing SUHF as a type of MCSCF, it has an incomplete active space, where all N_e electrons are correlated in N_e active orbitals, while there is an intrinsic secondary space whose occupations are strictly zero.[22] Thus, there are fewer double excitation sub-blocks to be considered than in other MRPT2 schemes, and they can be categorized as one of the following sub-blocks: fully internal, semi-external, and external excitations, where zero, one, and two electrons are excited to the virtual space, respectively. The fully internal excitations are those within the active space, and they are neglected in CASPT2[4,5] under the assumption that a CAS does not change in the presence of dynamical correlation. This type of excitation is also missing in other MRPT2 theories that use an incomplete model space[36−38] because it would give rise to significant complication or a large number of intruder states. The exclusion of fully internal excitations may be valid if the incomplete active space is almost complete. However, this is far from the case for SUHF. Therefore, one must consider excitations into almost fully occupied orbitals or from nearly empty ones, introducing significant redundancies. Given this fact, this "excitation-after-projection" scheme, as given in eq 21, is not advantageous because it is likely to introduce significant complication into the derivation whereas most fully internal excitations are redundant.

The above difficulty can be avoided by exploiting the compact representation of the SUHF wave function. Namely, in the "projection-after-excitation" *ansatz*, we write

$$|\Omega\rangle = \hat{P} \hat{a}_\Omega |\Phi_0\rangle \tag{22}$$

where broken-symmetry excitation operator $\hat{a}_\Omega$ generates a series of excited determinants with respect to $|\Phi_0\rangle$, such as $|\Phi_i^a\rangle$ and $|\Phi_{ij}^{ab}\rangle$, which are then projected by $\hat{P}$. Because there is a clear distinction between occupied and virtual orbitals in $|\Phi_0\rangle$, all $|\Omega\rangle$ are realistic with a large norm. Nevertheless, we should note that the projection-after-excitation basis is still slightly redundant due to the nature of $\hat{P}$, which includes not only excitations but also de-excitations.[27]

Using the shorthand $|\Phi_\mu\rangle = \hat{a}_\mu |\Phi_0\rangle$, we write the first-order wave function as

$$|\psi_1\rangle = \sum_{\mu} \hat{Q}_0 \hat{P} |\Phi_\mu\rangle t_\mu \tag{23}$$

It should be stressed that in the above equation, only projected singles and doubles are essential for expanding $|\psi_1\rangle$. The projected-excited determinants of higher rank could be included in $|\psi_1\rangle$ because they in fact interact with $\hat{P}|\Phi_0\rangle$ through $\hat{H}$. However, it is expected that their contributions should be negligible or even nonexistent as it can be easily shown that $\{\hat{P}|\Phi_i^a\rangle, \hat{P}|\Phi_{ij}^{ab}\rangle\}$ spans exactly the first-order interaction space with respect to $\hat{P}|\Phi_0\rangle$.[22] It is also noteworthy that the projected singles and doubles include the space corresponding to the fully internal excitations of the excitation-after-projection scheme and are thus potentially capable of relaxing the SUHF (incomplete) active space.

Using eq 23, the second-order energy can be given by

$$E_2 = \langle \psi_0 | \hat{H} | \psi_1 \rangle = \sum_{\mu}^{\text{SD}} \langle \Phi_0 | \hat{P} \hat{H} \hat{Q}_0 \hat{P} | \Phi_\mu \rangle t_\mu \tag{24}$$

which, noting that there is no contribution from singles due to the Brillouin theorem (eq 5), becomes

$$E_2 = \sum_{i>j} \sum_{a>b} \langle \Phi_0 | (\hat{H} - E_{\text{SUHF}}) \hat{P} | \Phi_{ij}^{ab} \rangle t_{ij}^{ab} \tag{25}$$

It should be pointed out that this expression is identical to that of the second-order energy of EMP2(0).[19] The amplitudes **t** are determined by projecting the first-order equation (eq 15) with the manifold $\{\hat{Q}_0 \hat{P} | \Phi_\mu \rangle\}$

$$\sum_{\nu}^{\text{SD}} \langle \Phi_\mu | \hat{P} \hat{Q}_0 (\hat{H}_0 - E_0) \hat{Q}_0 \hat{P} | \Phi_\nu \rangle t_\nu + \langle \Phi_\mu | \hat{P} \hat{Q}_0 \hat{H} \hat{P} | \Phi_0 \rangle = 0 \tag{26}$$

which can be simplified to

$$\sum_{\nu}^{\text{SD}} A_{\mu\nu} t_\nu + v_\mu = 0 \tag{27}$$

with

$$A_{\mu\nu} = \langle \Phi_\mu | \hat{P} \hat{Q}_0 (\hat{H}_0 - E_0) \hat{Q}_0 \hat{P} | \Phi_\nu \rangle \tag{28}$$

$$v_\mu = \langle \Phi_\mu | (\hat{H} - E_{\text{SUHF}}) \hat{P} | \Phi_0 \rangle \tag{29}$$

Thus, the linear equation depends on the choice of zeroth-order Hamiltonian $\hat{H}_0$. It is noteworthy that eq 27 resembles the amplitude equations of other MR methods. In these methods, the matrix that corresponds to **A** is often diagonalized in each excitation sub-block, which is feasible if 3RDM can be diagonalized.[5,36,37] The linear dependence is also removed through this procedure.[4] On the contrary, in our projection-after-excitation scheme, there appears to be no such separable sub-blocks of excitations, so **A** cannot be diagonalized. However, **A** is generally sparse regardless of the choice of $\hat{H}_0$[22] if the orbital set used is biorthogonal between α and β spins.[39] Also, the linear dependence in **A** shows up in **v** in exactly the same manner,[27,40] so it need not be removed in practice. Thus, linear equations (eq 27) can be directly solved.

We note that singles should be explicitly treated when solving eq 27. Otherwise, convergence is usually not obtained. This is because the projected singles and doubles are not orthogonal to each other (due to the redundancy in our scheme), and the linear dependence would not be treated correctly if without singles. In any case, the singles space is trivial in size and is required when the generalized Brillouin theorem is not satisfied, which is often the case in our illustrative calculations below. Therefore, we always include single excitations throughout this work.

It is well known that perturbation theory can be formulated as a variational problem.[29,30] Namely, one can define the Hylleraas functional

$$\mathcal{L} = \langle \psi_1 | (\hat{H}_0 - E_0) | \psi_1 \rangle + 2 \langle \psi_1 | \hat{H} | \psi_0 \rangle \tag{30}$$

whose stationary point corresponds to the second-order energy E_2. Equation 26 appears as a consequence of the variational principle of $\mathcal{L}$ with respect to the amplitudes. With $\mathcal{L}$, it is rather straightforward to adopt the standard derivative methods.[41,42]

Now that we have established a general perturbation theory with SUHF based on the projection-after-excitation scheme, only a definition of $\hat{H}_0$ is now required, which is somewhat arbitrary. Nevertheless, it is widely known that the choice of $\hat{H}_0$ significantly affects the final performance, and it should therefore be carefully chosen. To end this section, we remark on a few preferable conditions that $\hat{H}_0$ should hold:

(1) It must have $|\psi_0\rangle = \hat{P}|\Phi_0\rangle$ as its eigenstate. In this work, we employ a spin-free zeroth-order Hamiltonian so that $[\hat{H}_0, \hat{P}] = 0$, which allows for a considerable simplification, although this is by no means a requisite condition.

(2) It should be chosen such that the perturbation $\hat{V}$ is sufficiently small.

(3) It should be composed of one-electron operators for ease of derivation and computation.

(4) It should reduce to the standard Fock operator in the absence of $\hat{P}$ so as to reproduce the MPn energies.

In the following sections, we will consider two possibilities for the form of $\hat{H}_0$ based on these guidelines.

2.3. EMP2. The original EMP2(0) also starts with the same *ansatz* for $|\psi_1\rangle$, i.e., eq 23.[19] Without explicitly defining $\hat{H}_0$, its first-order wave function is fixed to the spin-projected MP1 wave function. The amplitudes are obtained by semi-canonicalization of spin-contaminated UHF-like Fock matrices, where one separately diagonalizes the occupied−occupied and virtual−virtual blocks of the spin-dependent Fock matrices computed with broken-symmetry $|\Phi_0\rangle$.[43] This circumvents iterative calculations when solving eq 26, which are otherwise necessary because $\hat{H}_0$ is generally not diagonal in the working basis $\{\hat{Q}_0 \hat{P} | \Phi_\mu \rangle\}$. While EMP2(0) does go back to standard MP2 when $\hat{P}$ is neglected, it remains largely unclear with respect to what energy **t** is optimized; hence, the derivation of analytical derivatives would become complicated.

A somewhat more general formalism can be derived by using the normal-ordered Hamiltonian in eq 8. The idea is to write the projected Hamiltonian $\hat{H}\hat{P}$ as

$$\hat{H}\hat{P} = \hat{\mathcal{H}}_0 + \hat{\mathcal{V}} \tag{31}$$

with

$$\hat{\mathcal{H}}_0 = \sum_g^{N_g} w_g \left(E_g \hat{R}_g + \sum_{pq} (\mathbf{F}_g)_{pq} \{\hat{a}_q^p\}_g \hat{R}_g \right) \tag{32}$$

$$\hat{\mathcal{V}} = \sum_g^{N_g} w_g \left(\frac{1}{4} \sum_{pqrs} \langle pq \| rs \rangle \{\hat{a}_{rs}^{pq}\}_g \hat{R}_g \right) \tag{33}$$

In our previous study on spin-extended CISD (ECISD),[22] it was found that the contribution of $\hat{\mathcal{V}}$ is typically small compared to that of $\hat{\mathcal{H}}_0$; thus, the latter was used as preconditioning in the iterative diagonalization of the ECISD Hamiltonian. This indicates that $\hat{\mathcal{H}}_0$ is reasonable for a zeroth-order component of the projected Hamiltonian. Because $\hat{\mathcal{H}}_0$ does not have $\hat{P}|\Phi\rangle$ as its eigenstate in general, one can formally define the following zeroth-order Hamiltonian for EMP2:

$$\hat{H}_0^{\text{EMP2}} = \hat{\mathcal{P}}_0 \hat{\mathcal{H}}_0 \hat{\mathcal{P}}_0 + \hat{Q}_0 \hat{\mathcal{H}}_0 \hat{Q}_0 \tag{34}$$

However, because $\hat{\mathcal{H}}_0$ is not spin-free, the matrix elements of $\hat{P}\hat{\mathcal{H}}_0\hat{P}$, including the zeroth-order energy

$$E_0^{\text{EMP2}} = \frac{\langle\Phi_0|\hat{P}\hat{\mathcal{H}}_0\hat{P}|\Phi_0\rangle}{\langle\Phi_0|\hat{P}|\Phi_0\rangle} \tag{35}$$

become cumbersome to evaluate; the required number of grid points becomes N_g^3, which adds considerable computational overhead. To alleviate this problem, we simply introduce the following approximation:

$$\langle\Phi_\mu|\hat{P}\hat{\mathcal{H}}_0\hat{P}|\Phi_\nu\rangle \approx \langle\Phi_\mu|\hat{\mathcal{H}}_0|\Phi_\nu\rangle \tag{36}$$

We deem this approximation to be reasonable because $\hat{\mathcal{H}}_0$ itself plays the role of approximate spin projection. In fact, if $\hat{V}$ is negligible, which is our assumption in EMP2, then $\hat{\mathcal{H}}_0 \approx \hat{H}\hat{P}$ and therefore eq 36 certainly holds. One caveat is that the perturbation series would not converge to the correct limit, eq 13. With eq 36, the zeroth-order energy E_0 is simply the SUHF energy. By absorbing E_{SUHF} in $\hat{\mathcal{H}}_0$ and defining

$$\hat{\bar{\mathcal{H}}}_0 = \sum_g^{N_g} w_g\left((E_g - E_{\text{SUHF}})\hat{R}_g + \sum_{pq}(\mathbf{F}_g)_{pq}\{\hat{a}_q^p\}_g\right) \tag{37}$$

the amplitude (eq 26) becomes

$$\sum_\nu^{\text{SD}}\left[\langle\Phi_\mu|\hat{\bar{\mathcal{H}}}_0|\Phi_\nu\rangle - \langle\Phi_\mu|\hat{\bar{\mathcal{H}}}_0|\Phi_0\rangle\langle\Phi_0|\hat{P}|\Phi_\nu\rangle - \langle\Phi_\mu|\hat{P}|\Phi_0\rangle\langle\Phi_0| \right.$$
$$\left. \hat{\bar{\mathcal{H}}}_0|\Phi_\nu\rangle\right]t_\nu + \langle\Phi_\mu|(\hat{H} - E_{\text{SUHF}})\hat{P}|\Phi_0\rangle = 0 \tag{38}$$

which means the matrix $\mathbf{A}$ can be expressed as

$$A_{\mu\nu}^{\text{EMP2}} = \langle\Phi_\mu|\hat{\bar{\mathcal{H}}}_0|\Phi_\nu\rangle - \langle\Phi_\mu|\hat{\bar{\mathcal{H}}}_0|\Phi_0\rangle\langle\Phi_0|\hat{P}|\Phi_\nu\rangle$$
$$- \langle\Phi_\mu|\hat{P}|\Phi_0\rangle\langle\Phi_0|\hat{\bar{\mathcal{H}}}_0|\Phi_\nu\rangle \tag{39}$$

Incidentally, we note that the EMP2(0) amplitudes can be obtained as a special case by assuming no rotation is done ($\hat{R}_g = \hat{1}$) in eq 38, i.e., no spin projection is performed. In such a case, one can easily find an orbital basis that diagonalizes the matrix elements in the first term of the equation: the semi-canonical orbital basis. On the other hand, this generalized EMP2 (eq 38) is nonorthogonal and contains off-diagonal elements; thus, it is solved iteratively as described in the previous section. The Hylleraas functional for EMP2 is straightforward to derive using these approximate matrix elements.

2.4. SUPT2. While the derivation of EMP2 in the previous section is largely specific to the nonorthogonal structure of $\hat{P}$, it is also interesting to incorporate and combine the conventional wisdom of established MR perturbation theories. To this end, we will closely follow the approach taken by CASPT2.[4,5] This perturbation scheme is therefore called SUPT2, and it is based upon the spin-average generalized Fock operator

$$\hat{F} = \sum_{PQ} f_{PQ}(\hat{a}_{Q\alpha}^{P\alpha} + \hat{a}_{Q\beta}^{P\beta}) \tag{40}$$

where the generalized Fock matrix $\mathbf{f}$ is given in the same manner as in CASPT2, i.e., through the 1RDM $\mathbf{D}$ of the reference wave function,

$$f_{PQ} = h_{PQ} + \sum_{RS} D_{SR}\left[\langle PR|QS\rangle - \frac{1}{2}\langle PR|SQ\rangle\right] \tag{41}$$

Then, a zeroth-order Hamiltonian may be defined as

$$\hat{H}_0 = \hat{\mathcal{P}}_0\hat{F}\hat{\mathcal{P}}_0 + \hat{Q}_0\hat{F}\hat{Q}_0 \tag{42}$$

The important point here is that $[\hat{F}, \hat{P}] = 0$, which allows for the desired eigenvalue equation,

$$\hat{H}_0\hat{P}|\Phi_0\rangle = E_0\hat{P}|\Phi_0\rangle \tag{43}$$

where the zeroth-order energy is

$$E_0 = \langle\Phi_0|\hat{F}\hat{P}|\Phi_0\rangle = \sum_{PQ} f_{PQ}D_{QP} \tag{44}$$

Using $\hat{H}_0\hat{\mathcal{P}}_0 \equiv E_0\hat{\mathcal{P}}_0$, it is easy to show that the $\mathbf{A}$ matrix in eq 29 is

$$A_{\mu\nu}^{\text{SUPT2}} = (F_{\mu\nu} - E_0 S_{\mu\nu}) - S_{\mu0}(F_{0\nu} - E_0 S_{0\nu})$$
$$- (F_{\mu0} - E_0 S_{\mu0})S_{0\nu} \tag{45}$$

with the projected matrix elements

$$F_{\mu\nu} = \langle\Phi_\mu|\hat{F}\hat{P}|\Phi_\nu\rangle \tag{46}$$

$$S_{\mu\nu} = \langle\Phi_\mu|\hat{P}|\Phi_\nu\rangle \tag{47}$$

which can be straightforwardly evaluated.

2.5. SUPT2 with a Shift Operator. In our preliminary calculations, it was found that SUPT2 suffers from intruder states. This happens whenever some eigenvalues of $\hat{H}_0$ in the orthonormal space, in which the overlap metric is diagonal, are nearly degenerate with E_0. The so-called intruder state problem is notoriously common in CASPT2, especially if the active space is small, and the de facto standard for ameliorating this issue is to shift the zeroth-order Hamiltonian by a real constant ϵ:[33]

$$\hat{H}_0 \rightarrow \hat{H}_0 + \epsilon\hat{Q}_0 \tag{48}$$

A typical choice for ϵ in CASPT2 is 0.2–0.3 hartree (E_H). It is also straightforward to use the above level-shifted $\hat{H}_0$ for SUPT2. E_2 of the real-shifted SUPT2 (rSUPT2) is underestimated because of the positive shift ϵ, but this is usually corrected by using the Hylleraas functional (eq 30) instead:

$$\mathcal{L}^{\text{rSUPT2}} = E_2 - \epsilon\langle\psi_1|\psi_1\rangle \tag{49}$$

As will be shown below, such a level shift mitigates the ill-behaved energy profiles of SUPT2. However, a real level shift merely moves the positions of singularities as the eigenvalues are likely to continuously change between negative and positive values when moving along a potential surface. Therefore, there is always a chance for divergence because the shifted eigenvalues can still be accidentally close to E_0. Prior to calculations, one does not know how large ϵ should be to guarantee that all eigenvalues are above E_0. Also, the level-shift corrected energy (eq 49) is not stationary with respect to the amplitudes, and its derivative requires appropriate Lagrange multipliers. One could simply use the uncorrected E_2, but it increasingly deteriorates with larger ϵ.

It is more appealing to use an imaginary level shift $i\epsilon$, which completely removes the singularities at the cost of a slight distortion in the potential surface.[34] With an imaginary level shift, the poles are shifted toward the imaginary axis and never appear on the real axis, on which one evaluates the energy. Another advantage of the imaginary level shift is that, away from the poles, the energy change induced by $i\epsilon$ is much smaller than that with the real level shift ϵ.[32,34] However, a disadvantage is that applying an imaginary shift to SUPT2 is not as straightforward because the original implementation for CASPT2 assumes an orthonormal basis, which is not tractable to compute in SUPT2. Below, we therefore formulate an imaginary level shift scheme in a slightly different way.

Suppose that we have successfully diagonalized the $\mathbf{A}$ matrix (which we never do in practice) and have obtained eigenvalues

$$\sum_\nu^{SD} A_{\mu\nu} U_{\nu\widetilde{\mu}} = \Delta_{\widetilde{\mu}} U_{\mu\widetilde{\mu}} \tag{50}$$

Note that in solving eq 50, linearly dependent solutions are discarded. Also, note that exactly the same redundancy is shared by v_μ. The unitary matrix $\mathbf{U}$ transforms $\{|\Phi_\mu\rangle\}$ to $\{|\widetilde{\Phi}_{\widetilde{\mu}}\rangle\}$ with

$$|\widetilde{\Phi}_{\widetilde{\mu}}\rangle = \sum_\mu^{SD} |\Phi_\mu\rangle U_{\mu\widetilde{\mu}} \tag{51}$$

which thus gives the following diagonal representation:

$$\langle \widetilde{\Phi}_{\widetilde{\mu}} | \hat{P}\hat{Q}_0(\hat{H}_0 - E_0)\hat{Q}_0\hat{P} | \widetilde{\Phi}_{\widetilde{\nu}} \rangle = \Delta_{\widetilde{\mu}} \delta_{\widetilde{\mu}\widetilde{\nu}} \tag{52}$$

Importantly, the projected basis $\{\hat{Q}_0\hat{P}|\widetilde{\Phi}_{\widetilde{\mu}}\rangle\}$ is *not* orthonormal. In other words, we skip the orthogonalization step employed in CASPT2 and directly diagonalize $\hat{P}\hat{Q}_0(\hat{H}_0 - E_0)\hat{Q}_0\hat{P}$ as a whole.

The amplitudes $T_{\widetilde{\mu}}$ in this diagonal basis are simply given by

$$T_{\widetilde{\mu}} = -\frac{V_{\widetilde{\mu}}}{\Delta_{\widetilde{\mu}}} \tag{53}$$

where

$$V_{\widetilde{\mu}} = \langle \widetilde{\Phi}_{\widetilde{\mu}} | \hat{P}\hat{Q}_0\hat{H}\hat{P} | \Phi_0 \rangle = \sum_\mu U_{\mu\widetilde{\mu}}^* v_\mu \tag{54}$$

Nearly zero $\Delta_{\widetilde{\mu}}$ (those not caused by the linear dependency) obviously gives rise to a divergence in the amplitudes and thus in the second-order energy. In the proposed imaginary-shifted SUPT2 (iSUPT2), the denominator is directly regularized by $i\epsilon$ instead of changing the zeroth-order Hamiltonian like in eq 48

$$T_{\widetilde{\mu}} \rightarrow -\frac{\langle \widetilde{\Phi}_{\widetilde{\mu}} | \hat{P}\hat{Q}_0\hat{H}\hat{P} | \Phi_0 \rangle}{\Delta_{\widetilde{\mu}} + i\epsilon} \tag{55}$$

where only the real part is used for the evaluation of the second-order energy in order to avoid complex algebra. Namely, our imaginary-shifted amplitudes are *defined* as

$$\mathcal{T}_{\widetilde{\mu}} \equiv -\frac{\langle \widetilde{\Phi}_{\widetilde{\mu}} | \hat{P}\hat{Q}_0\hat{H}\hat{P} | \Phi_0 \rangle \Delta_{\widetilde{\mu}}}{\Delta_{\widetilde{\mu}}^2 + \epsilon^2} \tag{56}$$

which are apparently singularity-free. To obtain the working amplitude equation, we back-transform eq 56 using eqs 50 and 51 to get

$$\sum_{\lambda\nu} A_{\mu\lambda} A_{\lambda\nu} t_\nu + \sum_\nu A_{\mu\nu} v_\nu + \epsilon^2 t_\mu = 0 \tag{57}$$

where we have used the unitarity of $\mathbf{U}$. The iSUPT2 energy is obtained by substituting the converged $\mathbf{t}$ into the Hylleraas functional. Again, such an energy is not stationary with respect to the amplitudes. The equation is quadratic in $\mathbf{A}$, but this can be easily handled by forming $\mathbf{Ax}$ twice, i.e., $\mathbf{At}$ followed by $\mathbf{A(At+v)}$. Hence, the computational cost is doubled, which is still much better than diagonalizing the entire matrix to compute $\Delta_{\widetilde{\mu}}$ explicitly.

We should stress that the above approach is different from the use of the modified zeroth-order Hamiltonian $\hat{H}_0 + i\epsilon\hat{Q}_0$. The former is deemed to be more beneficial because it does not require the diagonalization of the overlap matrix to obtain an orthonormal basis whereas the latter does. Nonetheless, this difference results in a very minor change in the final energy in our experience.

Finally, we note that EMP2 is almost always free from the intruder state problem because $\mathbf{A}$ is thought of as an approximation of the ECISD Hamiltonian, neglecting two-particle-like operator $\hat{\mathcal{V}}$. Hence, if the ground state is represented well by the reference SUHF at zeroth order, then the eigenvalues of $\mathbf{A}$ are expected to always be positive except for those resulting from redundancies.

3. COMPUTATIONAL DETAILS

In this section, we describe computational details. Symmetry-projected calculations were performed with the *GELLAN* suite of programs,[44] and SR (MP2, CCSD, and CCSD(T)) and CASPT2 calculations were carried out with *Gaussian*[45] and *Molpro*,[46] respectively. Since we deal with unrestricted determinants (i.e., eigenstates of $\hat{S}_z$), the integrations of α and γ can be performed analytically.[11,22] Hence, all calculations presented used $N_g = 4$ grid points only for the β rotations, which was found to be sufficient for obtaining numerically exact $\langle \hat{S}^2 \rangle$. Spatial symmetry is ensured by performing one-shot symmetry projection. For triplet calculations, typically high-spin states are found to be slightly more favorable than low-spin states, although the difference is usually negligible. In some cases, they cannot represent the correct spatial symmetry, and low-spin states are therefore used.

In EMP2 and SUPT2, we often employ the frozen core approximation, where core electrons are not correlated. This can be achieved by constrained SUHF (cSUHF),[22,47,48] where natural orbitals with the largest occupation numbers are obtained as doubly occupied closed-shell orbitals. To correctly specify the desired doubly occupied orbitals in the energetical order, we then form the generalized Fock matrix and diagonalize only in this closed-shell space. Note that the generalized Brillouin theorem is no longer satisfied for these orbitals, so single excitations are included in the evaluation of the second-order energy.

The linear equations of EMP2 and SUPT2 are solved with the direct inversion of iterative subspace (DIIS).[49,50] In each iteration, the computational complexity scales as $O(N_g N_o^2 N_v^3)$, where N_o and N_v are the numbers of occupied and virtual orbitals, respectively. Currently, we simply use diagonal elements for preconditioning, although this is not an optimal

choice. Therefore, the DIIS convergence is somewhat slow with the present implementation. Nevertheless, other preconditioning schemes are available to improve the convergence behavior,[24] and we will test and report their performances in a separate paper.

4. ILLUSTRATIVE CALCULATIONS

4.1. Single-Bond Dissociation: HF. We use the HF molecule as our first test case. The 6-31G basis set is used,[51] and the F 1s orbital is frozen. Figure 1 shows the energy
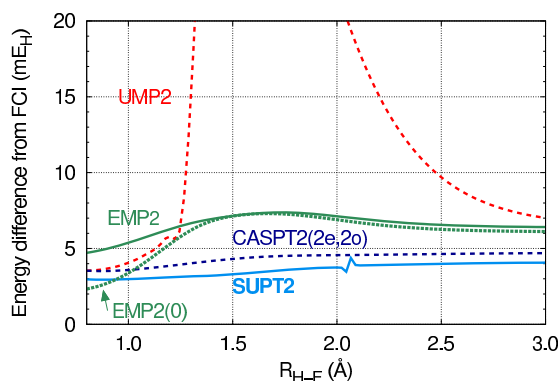
Figure 1. Energy difference $E - E_{FCI}$ in mE_H for several perturbation schemes in the HF potential energy curve computed with the 6-31G basis.

differences of several methods against FCI. As is well known, UMP2 gives a sharp derivative discontinuity at the Coulson–Fischer point, where a HF determinant breaks the spin symmetry. Passing this point, broken-symmetry UMP2 gives a substantial error and becomes completely unreliable. Interestingly, EMP2 and EMP2(0) are very similar in energy to each other, showing almost no improvement of the former. This similarity is also seen in many other cases, indicating that the broken-symmetry Fock matrix already well represents $\hat{H}_0$ used in EMP2. Still, in general, EMP2(0) gains more correlation energy around the equilibrium bond length (ca. 0.95 Å), while both EMP2(0) and EMP2 tend to become less accurate when a molecule is stretched. Therefore, overall, the potential energy curve of EMP2 is more parallel to FCI. As a matter of fact, the nonparallelity error (NPE), which is defined as the difference between the maximum and minimum errors from FCI, is 2.7 mE_H for EMP2 and 5.0 mE_H for EMP2(0).

Although EMP2 and EMP2(0) both outperform SUHF, whose NPE is 13.8 mE_H, their improvements are not impressive given that CASPT2 with the minimal active space of $(2e, 2o)$ for single-bond breaking is even more accurate with an NPE of 1.2 mE_H. Because CASSCF $(2e, 2o)$ is a subset of SUHF,[22,48] it is expected that a PT2 from SUHF is comparable to or better than CASPT2 $(2e, 2o)$. This is indeed the case for SUPT2, which gives fewer errors along the dissociation path. Although the SUPT2 curve looks encouraging, it turns out to be discontinuous at approximately 2.05 Å. To inspect the sudden change in energy, the eigenvalues $\Delta_{\bar{\mu}}$ of $\mathbf{A}$ are plotted in Figure 2. As can clearly be seen, one of the eigenvalues becomes negative at the said point, responsible for the divergence in the second-order energy. It is noteworthy that a negative denominator ($\Delta_{\bar{\mu}} < 0$) itself does *not* cause any problem but an eigenvalue crossing zero is what is at stake. The characteristic of this nearly zero eigenvalue is different
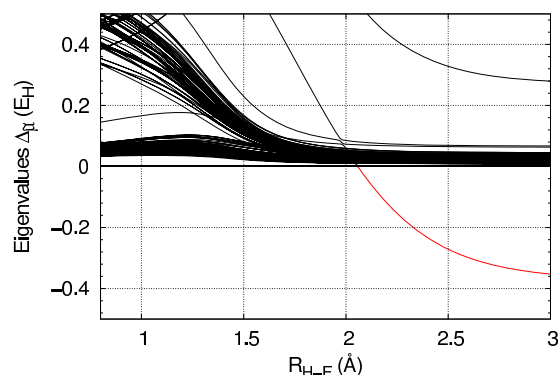

Figure 2. Eigenvalues $\Delta_{\bar{\mu}}$ of $\mathbf{A}$ for HF in SUPT2.

from that of other *essential* zero eigenvalues, which are caused by redundancies and can be easily removed because the corresponding $V_{\bar{\mu}}$ values are also exactly zero in eq 53.

Since CASPT2 $(2e, 2o)$ does not show such a divergence for this simple molecule, it is most likely that the intruder state in SUPT2 corresponds to fully internal excitations (ones within the active space) in CASPT2. In this sense, the intruder state problem seems more severe in SUPT2 than in CASPT2 because we never distinguish excitation classes in the former. To remove this intruder state from SUPT2, either a real level shift of $\epsilon \approx 0.2E_H$ or an imaginary level shift was required; otherwise, the energy divergence persists. In passing, as mentioned above, neither EMP2(0) nor EMP2 suffers from intruder states. Although the performance of SUPT2 is relatively satisfactory when the amplitudes are stable, the intruder state problem is a significantly unfavorable feature. In the next section, we will investigate this problem in more detail and show that the imaginary shift scheme appears to be the best compromise.

4.2. Multiple Bond Dissociation: H_2O and N_2. In this section, we focus on the symmetric dissociation of H_2O and the triple-bond breaking of N_2 as more complicated cases. Again, we use the 6-31G basis set and freeze the 1s orbitals of O and N as in the previous section.

In Figure 3, the energy error against FCI is plotted every 0.01 Å from $R_{O-H} = 0.8$ to 3.0 Å for the symmetric dissociation of H_2O. Most of the conclusions we drew in the previous section still hold here. The second-order energies computed with EMP2 and EMP2(0) are basically the same, but the latter is slightly larger at short bond lengths. Clearly, there are many more intruder states in SUPT2 compared to the case of the HF
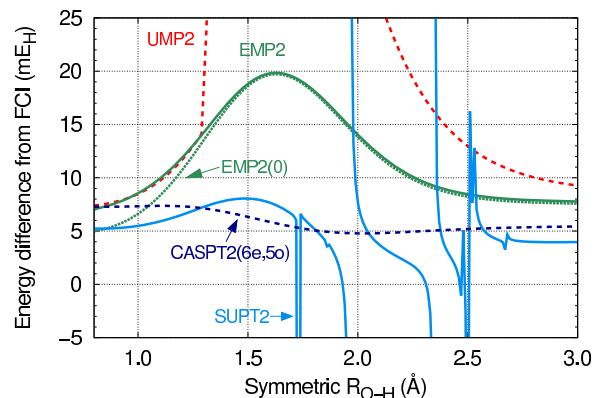
Figure 3. The same as for Figure 1 but for H_2O.

molecule, making its potential curve very unstable. Again, they can be understood as a divergence in amplitudes. To see this, the eigenvalue profile of **A** in SUPT2 for H_2O is plotted in Figure 4. Note that the discontinuous positions of SUPT2 in Figure 3 exactly correspond to the points where one of $\Delta_{\tilde{\mu}}$ crosses zero in Figure 4.
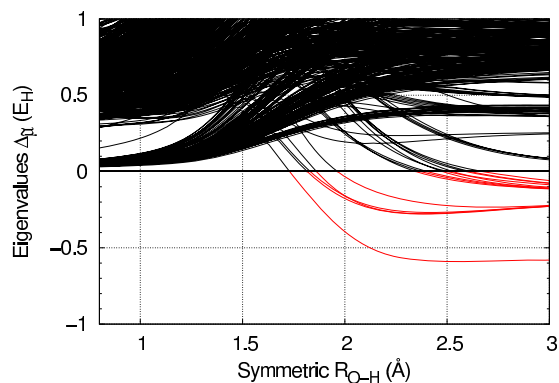

Figure 4. The same as for Figure 2 but for H_2O.

At this point, a remedy is indispensable to obtaining meaningful potential curves with SUPT2. We have tested real and imaginary level shifts with $\epsilon = 0.1E_H$, $0.2E_H$, $0.3E_H$, and $0.4E_H$ to alleviate the ill-behaved potential curve, and Figure 5

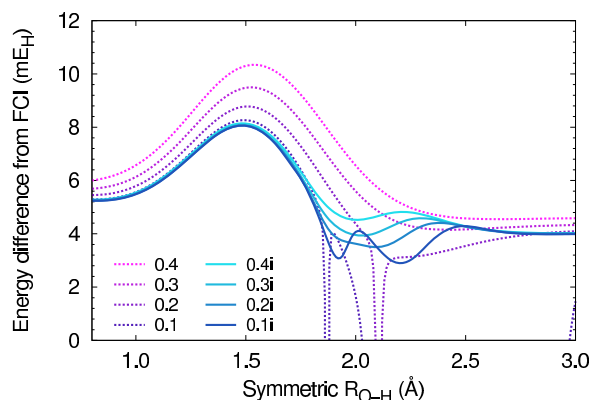**Figure 5.** Energy difference $E - E_{FCI}$ in mE_H for several level-shift values in the symmetric dissociation of H_2O. Red curves are real shifts, and blue curves are imaginary shifts. The second-order energy is corrected with eq 30.

shows their energy differences from FCI, where the level-shift corrected energy is evaluated according to eq 30. As expected, introducing a real level shift tends to quench the singularities as ϵ becomes larger, and it appears that $\epsilon = 0.3$ is sufficient to obtain a smooth curve for the present case. The second-order energy becomes slightly less accurate with ϵ, but this happens to a similar extent at all bond distances. In Table 1, we have tabulated the NPEs for the H_2O curves computed with the uncorrected and corrected second-order energies, E_2 and $\mathcal{L}$ (eqs 24 and 30). The level-shift correction is essential to retaining the qualitative results of rSUPT2. As such, we will report only the level-shift corrected energy $\mathcal{L}$ below, if not mentioned otherwise. However, for $\epsilon = 0.1$ and 0.2, the use of $\mathcal{L}$ does not cure the intruder state problem at all, and the divergent behavior is often amplified because $\langle \psi_1 | \psi_1 \rangle \gg 1$. Unfortunately, it is not possible to estimate a value that

Table 1. NPEs of Level-Shifted SUPT2 for the Symmetric Dissociation of H_2O (mE_H)

	uncorrected E_2		corrected $\mathcal{L}$	
ϵ/E_H	real	imag.	real	imag.
0.1	a	4.6	a	5.2
0.2	a	4.3	a	4.6
0.3	9.7	4.6	5.3	4.2
0.4	11.1	5.0	5.9	4.1
0.5	12.4	5.6	6.4	4.2
0.6	13.6	6.1	7.0	4.3

[a]Diverged.

removes all singularities in potential energy surfaces *a priori*; therefore, a trial-and-error approach is required.

In this regard, the imaginary shift scheme is more promising. It can be shown that, away from the singularities, the energy error induced by real ϵ is on the order of $\left(\dfrac{\epsilon}{\Delta_{\tilde{\mu}}}\right)$ for $\Delta_{\tilde{\mu}} \gg 1$, whereas that for imaginary $i\epsilon$ is $\left(\dfrac{\epsilon}{\Delta_{\tilde{\mu}}}\right)^4$.[32,34,52] Furthermore, the imaginary level shift is singularity-free. All of these features are illustrated in Figure 5, where the results for $i\epsilon = 0.1i$, $0.2i$, $0.3i$, and $0.4i$ are all continuous and smooth. The energy error does not grow with an increase in ϵ as significantly as for the real shift. As a result, NPEs are all reasonable for different $i\epsilon$ values with iSUPT2 (Table 1). Still, as can be seen, ϵ should not be too small or too large in the imaginary shift scheme, and the recommended value range is $i\epsilon = 0.3i-0.5i$.

Now we turn our attention to N_2. This molecule is more challenging than HF and H_2O and has been used to benchmark several MR methods.[21,34,53−56] The upper panel of Figure 6 shows the potential energy curves computed by
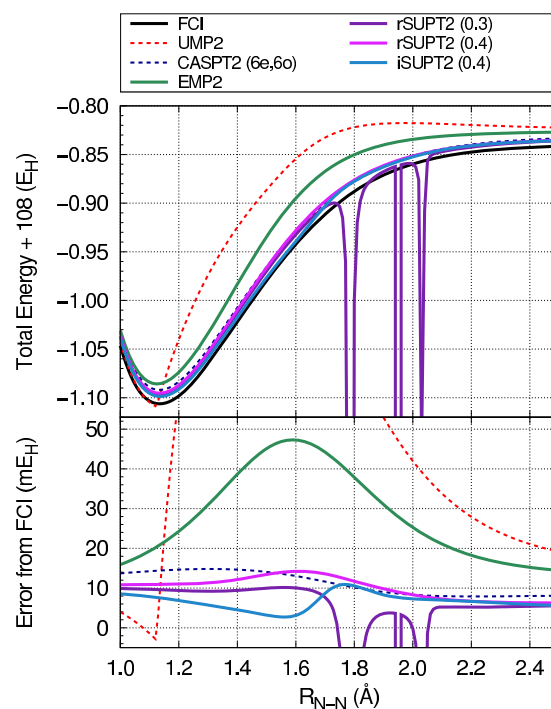

Figure 6. (Upper panel) Potential energy curves of N_2 computed with several methods using the 6-31G basis. (Lower panel) Energy error from FCI.

Table 2. Comparison of Several Methods for NPEs of HF, H$_2$O, and N$_2$ with Respect to FCI (mE$_H$)

	UMP2	CASPT2[a]	SUHF	EMP2(0)	EMP2	rSUPT2[b]	iSUPT2[c]	ECISD
HF	39.3	1.2	13.8	5.0	2.7	1.1	1.1	0.9
H$_2$O	66.2	2.6	67.9	14.7	12.8	5.3	4.1	3.8
N$_2$	100.2	6.9	104.1	38.0	35.1	8.0	8.2	15.6

[a]Active space: (2e, 2o) for HF, (6e, 5o) for H$_2$O, and (6e, 6o) for N$_2$. [b]Level-shift values: 0.2, 0.3, and 0.4 for HF, H$_2$O, and N$_2$, respectively. [c]Level-shift value: 0.4i for all molecules.

FCI and different PT2 schemes, where we have used an active space of (6e, 6o) for CASPT2 and employed ϵ = 0.3, 0.4 and iϵ = 0.4i for the level shift in SUPT2. We omit EMP2(0) because its energy is almost identical to that of EMP2. For the real-shifted SUPT2, ϵ = 0.4 is needed to remove all singularities. Therefore, with a real shift of ϵ = 0.3, SUPT2 produces pronounced peaks. Once an appropriate value is used to eliminate singularities, real- and imaginary-shifted SUPT2 are similar in performance, and their potential energy curves are almost indistinguishable from each other. In the lower panel of Figure 6, we have plotted the energy differences from FCI for N$_2$. For ϵ = 0.4 and iϵ = 0.4i, the errors of SUPT2 in considerably smaller than those in EMP2. The correlation energies obtained with these level shifts are akin to those of CASPT2, giving a satisfactory description of triple-bond breaking.

Finally, we close this section by summarizing the NPEs of HF, H$_2$O, and N$_2$ for each method with 6-31G in Table 2. From the table, the remarkable strength of SUPT2 should be clear; although it requires a proper treatment of singularities, the level-shifted SUPT2 rivals CASPT2 in accuracy. For N$_2$, SUPT2 even outperforms ECISD at only a fractional computational cost, indicating its potential. In particular, iSUPT2 is more advantageous than rSUPT2 in that it is capable of removing all singularities independently of ϵ.

4.3. Spectroscopic Constants of N$_2$. While we have seen that both EMP2 and SUPT2 can treat both static and dynamical correlation effects reasonably well and can describe molecular dissociations, it is also important for them to be able to predict molecular properties, such as spectroscopic constants. For this purpose, we continue to use the N$_2$ molecule as the test system. We employed the aug-cc-pVQZ basis[57] to compute the equilibrium bond length R_e, vibrational frequency ω_e, and dissociation energy D_e and compared the results with experiments.[58] Although D_e is calculated by the supermolecular approach (i.e., $D_e = E[100 \text{ Å}] - E[R_e]$), the size-consistency errors ($E[100 \text{ Å}] - 2E[\text{atom}]$ where quartet spin-projection is performed for atoms) are less than 0.02 kcal/mol for all methods. The almost negligible size-consistency errors might come as a surprise but are attributed to the character of the underlying broken-symmetry UHF determinant $|\Phi_0\rangle$ at the dissociation limit, which is a mixture of singlet, triplet, quintet, and septet, all nearly degenerate in energy. Since UHF is known to be size-consistent for the N$_2$ dissociation into two quartet atoms, which have almost no spin contamination, the singlet SUHF energy is naturally very close to the sum of the septet spin-projected atoms. This is how SUHF breaks valence bonds in general.

As shown in Table 3, as expected, CCSD(T) is most accurate and achieves "chemical accuracy" for all constants.[59] Although MP2 shows improvements over HF, it turns out that it overestimates the correlation energy ($E[R_e]$ = $-109.39369E_H$), as is evident from the CCSD energy ($E[R_e]$ = $-109.38684E_H$). Consequently, the equilibrium bond length

Table 3. Spectroscopic Constants of N$_2$ Computed with the aug-cc-pVQZ Basis Set

method	R_e/Å	ω_e/cm^{-1}	D_e/kcal mol^{-1}	$E[R_e]/E_H$
HF	1.066	2729	122.0	−108.99493
MP2	1.111	2202	236.5	−109.39369
CCSD	1.093	2434	214.4	−109.38684
CCSD(T)	1.100	2355	223.5	−109.40724
SUHF	1.090	2410	159.1	−109.06489
EMP2(0)	1.090	2471	223.4	−109.37420
EMP2	1.092	2453	222.4	−109.37291
rSUPT2 (0.25)	1.102	2330	214.5	−109.38428
iSUPT2 (0.4)	1.102	2317	214.5	−109.38589
CASSCF (6e, 6o)	1.102	2351	205.4	−109.12770
CASPT2 (6e, 6o)	1.101	2334	215.1	−109.38520
exp	1.098	2359	228.4	

and dissociation energy are also overestimated by 0.013 Å and 8.1 kcal/mol, respectively. The vibrational frequency ω_e is largely underestimated by 137 cm^{-1}. From these results, it is concluded that the MP2 level of theory is insufficient to describe the equilibrium of N$_2$.

It is found that both SUHF and CASSCF (6e, 6o) yield results far better than those of HF, indicating that it is quite advantageous to treat N$_2$ with a multideterminant wave function, even at equilibrium. SUHF is still less accurate than CASSCF (6e, 6o) because it lacks some dynamical correlation within the incomplete active space. This fact is directly reflected in their energy difference, which is more than 60 mE$_H$. However, SUPT2's ability to treat fully internal excitations means that it is able to capture the missing dynamical correlation at zeroth order; with a level shift of 0.4i, SUPT2 delivers a total energy very similar to that of CASPT2. The computed spectroscopic constants are in excellent agreement between these methods. They also resemble CCSD, although ω_e predicted by CCSD is inferior to those by predicted by iSUPT2 and CASPT2 (6e, 6o). We find that rSUPT2 with ϵ = 0.25 also gives almost the same results as these methods, including the total energy; however, its potential curve contains a few singularities, rendering its applicability somewhat questionable.

EMP2(0) and EMP2 produce smaller correlation energies at equilibrium than SUPT2 and CASPT2, by ca. 10mE$_H$; however, at the dissociation limit, their energies are even more underestimated, and the computed D_e's therefore happen to be in better agreement with the experimental value. Nonetheless, it is clear that their descriptions are not satisfactory for R_e, which show almost no improvement over SUHF. The computed ω_e are even worse than that of SUHF. Overall, SUPT2 with an appropriate level shift prevails over EMP2(0) and EMP2 in predicting the spectroscopic constants of N$_2$.

4.4. Singlet−Triplet Splitting Energies. Excitation energy is an important quantity. There are approaches to

Table 4. Computed Singlet−Triplet Gaps of Small Systems in kcal/mol

method	C	O	Si	NH	OH$^+$	O$_2$	NF	ME	MAE
CASPT2 ($2e$, $2o$)	29.1	45.5	17.5	36.5	49.8	15.4	32.0	−1.3	1.6
CASPT2 (FV)	29.1	45.5	17.4	37.0	50.2	22.8	32.2	−0.1	0.6
SUHF	22.3	38.7	8.3	32.7	45.2	26.0	31.6	−4.3	5.3
EMP2(0)	29.1	45.4	17.2	35.8	49.3	25.2	34.4	0.2	0.6
EMP2	29.1	45.3	17.3	35.7	49.1	24.9	33.9	0.1	0.7
SUPT2	29.7	46.2	17.8	36.7	50.5	24.3	34.1	0.6	0.7
rSUPT2 (0.25)	29.6	46.2	17.5	36.7	50.5	24.6	34.2	0.6	0.7
iSUPT2 (0.4)	29.7	46.2	17.6	36.8	50.5	24.2	34.2	0.6	0.6
exp	29.1	45.2	17.3	35.9	50.5	22.6	34.3		

treating excited states based on the PHF framework, such as linear-response theory[20] and nonorthogonal CI.[60] However, since our PT2 methods are currently formulated in a state-specific way, it is not straightforward to apply them to excited states. Having said that, it is relatively easy to calculate the lowest state of a given spin symmetry.

Recently, Rivero et al. benchmarked singlet−triplet splitting energies with several PHF methods, including SUHF.[61] They showed that while SUHF's results are reasonable, further improvements can be achieved by breaking and restoring a variety of other symmetries, such as $\hat{S}_z$. This means that a balanced treatment of static and dynamical correlation effects is important for predicting accurate singlet−triplet gaps. Hence, it is interesting to ask how much advantage our second-order perturbation theories bring about in computing this quantity.

4.4.1. Atoms and Diatomic Molecules. We first compute the ST splitting energies of atoms (C, O, and Si) and diatomic molecules (NH, OH$^+$, O$_2$, and NF). We use the aug-cc-pVQZ basis and the experimental geometries for the molecules.[62] All electrons are correlated in our calculations. For these atoms, the ground state is a triplet ^3P state, whereas the lowest singlet state is ^1D. For the molecules, we compute the adiabatic excitation energies of $^3\Sigma \rightarrow {}^1\Delta$. The biradical nature of these systems poses a challenge for SR methods because their singlet states are qualitatively represented by two determinants, meaning very demanding triples are required for quantitative accuracy. Consequently, standard post-HF methods, such as MP2 and CCSD, significantly overestimate the ST gaps.[19]

Table 4 presents the calculated ST gaps together with the mean errors (MEs) and mean absolute errors (MAEs) against the experimental values. We have used two active spaces for CASPT2: ($2e$, $2o$) and full-valence (FV) spaces. The former is the minimum space required to treat (two-determinant) biradical systems, and triplet states are simply a single determinant of restricted open-shell HF. From the table, it is immediately clear that this small active space is not sufficient for the ST gap of O$_2$; the predicted value is 15.4 kcal/mol, and the error against the experimental value (22.6 kcal/mol) is 7.2 kcal/mol. The rather large error is ascribed to the fact that both singlet and triplet states are overly correlated in this system with CASPT2 ($2e$, $2o$). This imbalance was not fixed by a level shift; CASPT2 ($2e$, $2o$) with $\epsilon = 0.25$ still gave an ST gap of 15.8 kcal/mol. On the other hand, CASPT2 with full-valence active space ($12e$, $8o$) yields an excellent result of 22.8 kcal/mol. Overall, the MAE of FV-CASPT2 is 0.6 kcal/mol, whereas that of CASPT2 ($2e$, $2o$) is 1.6 kcal/mol. However, it is apparent that it might not always be feasible to employ a full-valence active space. It is important to select active orbitals that are physically relevant, but they depend on various factors such

as geometry and chemical reactions in question. After all, it still remains difficult to construct an appropriate active space, although many authors have suggested practical ways to ease this task.[63−68]

SUHF does not usually require an active space to be chosen (except for the specification of core orbitals) and is therefore more flexible in this sense. For these rather simple examples, we found that all PT2 schemes based on SUHF delivered similarly accurate descriptions. The difference between EMP2(0) and EMP2 is almost negligible, as was seen in the previous sections, and both achieved accuracies similar to that of FV-CASPT2. The maximum errors were obtained for O$_2$, but they are less than those of CASPT2 ($2e$, $2o$): +2.6 and +2.3 kcal/mol for EMP2(0) and EMP2, respectively. The chief difference between SUHF and CASSCF ($2e$, $2o$) in this system is that the antibonding π_g orbitals are fractionally occupied in the former. The natural occupation numbers of SUHF are 0.012 and 0.031 for the singlet and triplet, respectively, implying that there is some contribution to the static correlation that the minimum active space was not able to capture in CASSCF ($2e$, $2o$).

For the tested systems, the SUPT2 amplitudes are stable without a level shift, and we can thus investigate the accuracy that the original SUPT2 potentially has to offer. For comparison, we have carried out SUPT2 calculations with three different level-shift conditions: $\epsilon = 0$, 0.25 and $i\epsilon = 0.4i$. As can be seen from Table 4, SUPT2 without a level shift provides results as accurate as EMP2. Evidently, the accuracy of SUPT2 is almost unchanged when a level shift is introduced. The energy deviation caused by a level shift occurs in a balanced manner between singlet and triplet states (less than a few mE_H in all cases) such that the influence on the calculated excitation energy is negligible.

Overall, both EMP2 and SUPT2 can successfully predict the ST gaps for the systems tested here, while CASPT2 is also accurate if the active space is properly chosen. However, for more complicated systems, EMP2 and SUPT2 show different trends, as will be demonstrated below.

4.4.2. Transition-Metal Complexes. Transition-metal complexes are challenging not only for SR methods but also for MRPT2 because the results typically depend on the choice of active orbitals. Here, we report the results of our methods on ferrocene Fe(C$_5$H$_5$)$_2$ and [Fe(NO)(CO)$_3$]$^-$ and compare the ST gaps with strongly contracted N-electron valence state PT2 (NEVPT2).[71−73] The geometries were taken from refs 74 and 70, respectively. We used the cc-pVTZ basis set and froze the 1s orbitals of C, N, and O and the 1s, 2s, 2p, 3s, and 3p orbitals of Fe in the PT2 calculations. Relativistic effects were not accounted for in this study because it has been reported that they do not significantly affect the results.[68]

For ferrocene, the singlet state is dominated by a single configuration of Fe d^6. The lowest triplet state is doubly degenerate $^3E_1''$, mainly characterized as the d–d transitions from (d_{xy}, $d_{x^2−y^2}$) to (d_{xz}, d_{yz}).[75] Symmetry breaking and restoration within SUHF results in a triplet state that is dominantly $^3E_1''$ but is slightly mixed with E_1' spatial symmetry. We performed SUHF followed by spin-constrained SCF calculations (cSUHF), where we optimized SUHF orbitals such that the lowest 42 and 43 orbitals were doubly occupied in the singlet and triplet states, respectively.

For complex anion [Fe(NO)(CO)$_3$]$^−$, both the singlet ground state and lowest triplet state ($^3A_1$) are strongly correlated. A previous study indicated that the strong electron correlation arises from two degenerate bonding and antibonding orbital pairs, mainly composed of Fe d and NO π^*.[76] In particular, the $^3A_1$ state cannot be described by a single determinant in principle. We used a low-spin representation of SUHF to treat this triplet state. Constrained optimization was conducted to yield 37 doubly occupied orbitals.

Table 5 lists the ST gaps computed with various methods. As mentioned above, ferrocene may be reasonably treated with

Table 5. Lowest Singlet−Triplet Excitation Energies for Transition-Metal Complexes (eV)

| | ferrocene | [Fe(NO)(CO)$_3$]$^−$ |
	$^3E_1''$	$^3A_1$
HF	0.02	
MP2	1.98	
CASSCF[a]	0.97[b], 1.91[c]	2.27[d], 1.76[e], 2.44[f]
NEVPT2[a]	1.88[b], 2.09[c]	2.63[d], 3.40[e], 2.43[f]
SUHF	2.03	3.30
EMP2	1.47	1.25
iSUPT2[g]	1.59	2.63
ref	1.74[h]	2.32[i]

[a]Taken from ref 68. [b]Active space of (10e, 7o). [c]Active space of (18e, 15o). [d]Active space of (10e, 8o). [e]Active space of (14e, 9o). [f]Active space of (16e, 14o). [g]Imaginary shift of 0.4i E_H. [h]Experimental value from ref 69. [i]MRCI+Q with an active space of (14e, 9o), consisting of Fe d orbitals and the NO π and π^* orbitals.[70]

SR methods.[74,75] Indeed, although the predicted ST gap is much too small at the mean-field HF level of theory (0.02 eV), the MP2 dynamical correlation brings about significant improvement, yielding 1.98 eV, which is in good agreement with the experimental value of 1.74 eV.[69] However, [Fe(NO)(CO)$_3$]$^−$ requires a multireference treatment, and we were not able to obtain an ST gap with these methods.

Several active spaces were tested for CASSCF and NEVPT2 in ref 68, to which the reader is referred for more details about the active spaces used. As can be seen, the NEVPT2 results are mostly accurate, except for [Fe(NO)(CO)$_3$]$^−$ with (14e, 9o), which results in a gap of 3.40 eV (the reference value of MRCI+Q is 2.32 eV). This indicates the importance of selecting appropriate active orbitals.

For mean-field theory, SUHF drastically improves the ST gap of ferrocene on HF. We found that SUHF gains some portion of dynamical correlation, especially in the singlet ground state, resulting in a good opening of the ST gap (2.03 eV). However, as SUHF overestimates the gap by approximately 1 eV for the [Fe(NO)(CO)$_3$]$^−$ complex, a balanced description between static and dynamical correlations is necessary. The dynamical correlation effects of EMP2 and

SUPT2 tend to close the gap of SUHF. This is in contrast with the correlation effect of MP2 and NEVPT2, both of which predict larger gaps than their zeroth-order treatments. For both systems, EMP2 overcorrects the gap from SUHF, especially for [Fe(NO)(CO)$_3$]$^−$, where the gap is underestimated by more than 1 eV. On the other hand, SUPT2 with an imaginary shift of 0.4i offers accurate gaps compared to both SUHF and EMP2. Its results are also comparable to those of the highly sophisticated NEVPT2 approach. Finally, we have not tested EMP2(0) and rSUPT2, but we expect their results to be similar to those of EMP2 and iSUPT2, respectively.

4.5. Chromium Dimer. Describing the electronic structure of Cr$_2$ is notoriously challenging not only because it requires a considerable amount of static correlation at equilibrium but also because dynamical correlation plays a significant role. For this reason, only by highly sophisticated methods can its potential energy curve be computed with qualitative accuracy.[10,33,77−85] It is well known that the experimental potential energy curve of Cr$_2$ has a double-well structure;[86] the first deep minimum corresponds to 3d−3d bonding, and the shallow, shelf-like region is ascribed to the dissociation of the 4sσ bond. Therefore, it is critical for a zeroth-order reference wave function to be capable of capturing these different bonding effects.

Whether a method can describe such bonding effects is ensured by computing natural occupation numbers. The left and right panels of Figure 7 show the natural occupation
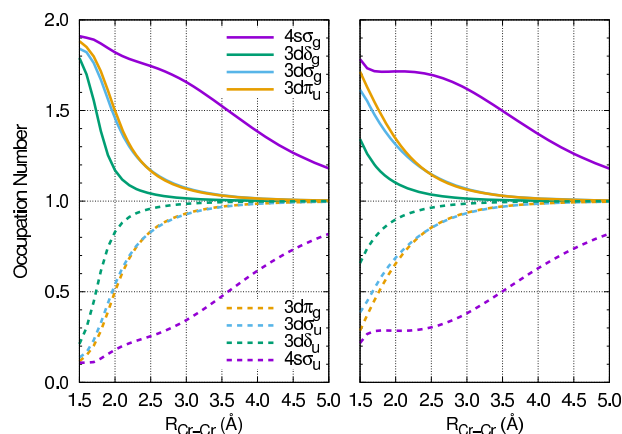
Figure 7. Natural occupation numbers of Cr$_2$ with CASSCF (12e, 12o) (left) and SUHF (right).

numbers of CASSCF (12e, 12o) and SUHF, respectively, computed with cc-pVQZ as a function of bond length. In both methods, the occupation numbers of the 4sσ_g and σ_u orbitals slowly decay to one (which corresponds to bond dissociation), while those of the 3d bonding and antibonding orbitals show a rapid decay. Thus, SUHF gives a qualitatively correct description. Seemingly, the 3d occupation numbers of SUHF are more fractional (closer to one) than those of CASSCF at a short distance. This is attributed to the dynamical correlation effect captured within the CAS, which is mostly neglected in SUHF. For instance, the SUHF energy at $R = 1.6$ Å is higher than the CASSCF energy by 143 mE_H, which is nevertheless reasonable given the N$_2$ case where SUHF misses a dynamical correlation energy of 60 mE_H (Section 4.3). Importantly, it is expected that the fully internal excitations in post-SUHF should exert their effectiveness for the missing dynamical correlation. Hence, with an appropriate post-SUHF scheme,

one can expect to obtain a qualitatively correct potential energy curve of Cr_2.

In Figure 8, the potential energy curves of Cr_2 are plotted for several methods using the cc-pVQZ basis set. Here, 3p and 3d
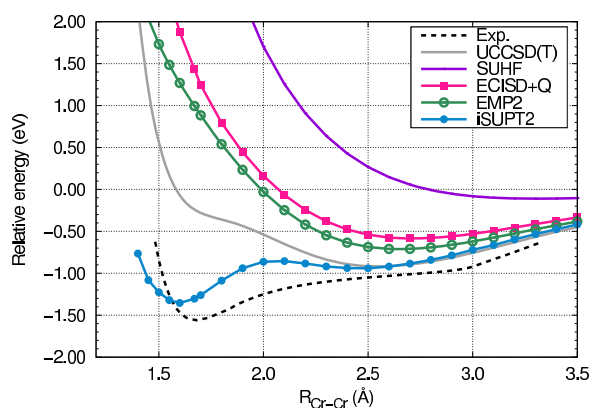

Figure 8. Potential energy curves of Cr_2.

electrons are correlated, and no relativistic effect is taken into account. For spin-projection methods, we used 18 doubly occupied orbitals. As expected, the SUHF curve is dissociative, meaning that a proper treatment of dynamical correlation is indispensable. The results of UCCSD(T), EMP2, and ECISD +Q are all disappointing, and they fail to predict the first minimum. On the other hand, it is intriguing that, unlike EMP2, the imaginary-shifted SUPT2 with $i\epsilon$ = 0.4i accounts for a large amount of dynamical correlation near the experimental equilibrium bond length R_e = 1.68 Å, producing the global minimum. Although the predicted bond distance is underestimated (R_e = 1.60 Å), the double-well shape is well captured, and the computed dissociation energy of D_e = 1.36 eV is also comparable to the experimental estimate of 1.45−1.56 eV.[10,87−89] For a more detailed comparison, it is highly desirable to include the relativistic effect and to investigate the convergence in basis set size, which we plan to report in future work.

Finally, it is argued that CASPT2 (12e, 12o) is not sufficient enough for Cr_2, and an active space of (12e, 28o) is needed for a quantitative description.[10] The limitation of SUPT2 is that its zeroth-order reference SUHF is not systematically improvable, unlike CASSCF, and our SUPT2 results therefore certainly cannot be made comparable to those of highly accurate CASPT2 (12e, 28o). However, it is highly probable that the use of spin-projected generalized HF (SGHF), in which further symmetry breaking and restoration of $\hat{S}_z$ is carried out, will bring significant improvements over SUPT2, and it is thus interesting to pursue this direction in the future. In any case, the above results for Cr_2 clearly indicate the superiority of SUPT2 compared to EMP2 and CI.

5. DISCUSSION

That EMP2 becomes inferior for more strongly correlated systems is indicative of the fact that the excitations relevant to entangled (most symmetry-broken) orbitals are not treated as properly as in SUPT2. To investigate this implication, we have carried out the energy decomposition analysis for EMP2 and SUPT2 based on the double-excitation class. To this end, we separate the SUHF natural orbital space into core (c), active (a), and virtual (v) spaces using appropriate occupation-

number thresholds. Although the nonorthogonal nature of these excitations may not allow for the rigorous quantification of their contributions because one cannot completely separate them in principle (especially if the Hylleraas functional is used to evaluate the energy), it is helpful to point out, even roughly, where the main difference between EMP2 and SUPT2 comes from.

In cases where an SUHF wave function is a better *ansatz* than that of CASSCF, SUPT2 is expected to offer more accurate results than CASPT2. We have already seen this for the HF molecule in Section 4.1 (CASSCF(2e, 2o) is a subset of SUHF). In this system, there are two active orbitals, and the energy contribution from the fully internal double excitation, (a, a) → (a, a), is found to be negligible in both EMP2 and SUPT2 as expected. The total energy difference of 2−4 mE_H between the two methods is mainly attributed to the following two excitation classes: (c, a) → (v, a) and (c, a) → (v, v). For other excitations, either the energy contribution is virtually zero or EMP2 and SUPT2 show almost identical energy contributions.

In general, the active space of SUHF is incomplete and is thought of as an approximation to CAS. Therefore, the fully internal excitations in EMP2 and SUPT2 should play a vital role, perturbatively correcting the active space of SUHF. We argue that such a correction can be valid if the character of the SUHF active space is reasonably close to CAS. However, whether the correction is accurate also depends on the choice of the zeroth-order Hamiltonian. We found that, in most cases such as N_2, there is an appreciable difference between EMP2 and SUPT2 in the treatment of the fully internal excitations. While these excitations capture a reasonable amount of correlation effects in SUPT2 and offer an improved approximation to CAS, they are not properly accounted for in EMP2. Although the contributions of other excitations such as (c, a) → (v, a) are also constantly underestimated in EMP2 compared to in SUPT2, they are relatively insignificant. The different treatments of the perturbative correction within the active space are the dominant contribution to the total energy difference, and it is concluded that the rather inferior behavior of EMP2 is attributed to the less accurate description of fully internal excitations.

6. CONCLUSIONS

In this article, we described second-order perturbation schemes with respect to spin-projected HF. The zeroth-order Hamiltonian of EMP2 was prepared as the Fock-like component of the projected Hamiltonian at each spin-rotation angle, whereas SUPT2 employed the generalized Fock operator constructed from the SUHF density matrix. The latter method almost always suffers from the intruder state problem, and we have discussed how one can remove singularities in practice by applying the level shift approach, especially with an imaginary shift value. These methods, together with the previously developed PT2, EMP2(0), were tested for several systems, including transition-metal complexes. In general, the imaginary-shifted SUPT2 showed the best performance. It yielded potential curves that are reasonably parallel to those of FCI, and the computed singlet−triplet gaps were in good agreement with experimental values. We were also able to obtain a qualitative description of the Cr_2 molecule with SUPT2. On the other hand, the description of the fully internal space in EMP2 is not satisfactorily accurate for difficult cases, such as multiple

bond dissociations and the spin gap of $[Fe(NO)(CO)_3]^-$. We therefore conclude that EMP2 is likely best for biradicaloid systems and that SUPT2 stands as a preferable perturbative correction to SUHF.

With the good performance of SUPT2 demonstrated in this work, it is interesting to ask whether its accuracy still holds for the prediction of molecular properties. Our initial results for the spectroscopic constants of N_2 are encouraging and support the validity of the SUPT2 method for such calculations. Computing molecular properties generally involves the relaxed density matrix and thus the derivatives of the total energy. Unfortunately, the level-shifted SUPT2 energy is not stationary with respect to the amplitudes. However, it is expected that the energy derivatives can be straightforwardly obtained by constructing an appropriate Lagrangian.[32,90] We are currently working on this task.

To achieve further quantitative accuracy, SUPT2 can be straightforwardly extended to SGPT2, second-order perturbation theory with SGHF. It has been shown that SGHF fixes many problems inherent in SUHF and produces more accurate wave functions and energy.[11,61] However, there are some additional complications that have to be addressed carefully, such as the treatment of the more general form of $\hat{P}$ in SGHF[11] as well as the convergence of linear equations (eq 27) with $\mathbf{A}$ that is presumably dense in SGPT2.

Other important developments include the generalization of our methods to excited states. In the present work, ground and excited states were treated separately in a state-specific manner. This clearly has a limitation in treating higher excited states and quasi-degenerate states, for which a multistate formulation is required. Because SUHF uses a single (broken-symmetry) determinant, the single-particle picture is not completely lost. Indeed, we have exploited this fact when constructing the first-order wave function *ansatz* in this work. Hence, we are hopeful that it is not difficult to extend our schemes to excited states by combining with existing SR approaches, such as a second-order perturbative correction on CIS.[91]

■ AUTHOR INFORMATION

Corresponding Author

*E-mail: tsuchimochi@gmail.com.

ORCID ⓘ

Takashi Tsuchimochi: 0000-0002-6378-1268

Notes

The authors declare no competing financial interest.

■ ACKNOWLEDGMENTS

■ REFERENCES

(1) Møller, C.; Plesset, M. S. Note on an Approximation Treatment for Many-Electron Systems. *Phys. Rev.* **1934**, *46*, 618−622.

(2) Bartlett, R. J. Many-Body Perturbation Theory and Coupled Cluster Theory for Electron Correlation in Molecules. *Annu. Rev. Phys. Chem.* **1981**, *32*, 359−401.

(3) Bartlett, R. J.; Musiał, M. Coupled-cluster theory in quantum chemistry. *Rev. Mod. Phys.* **2007**, *79*, 291.

(4) Andersson, K.; Malmqvist, P.-Å.; Roos, B. O.; Sadlej, A. J.; Wolinski, K. Second-order perturbation theory with a CASSCF reference function. *J. Phys. Chem.* **1990**, *94*, 5483−5488.

(5) Andersson, K.; Malmqvist, P.-Å.; Roos, B. O. Second-order perturbation theory with a complete active space self-consistent field reference function. *J. Chem. Phys.* **1992**, *96*, 1218−1226.

(6) Werner, H.-J.; Knowles, P. J. An efficient internally contracted multiconfiguration-reference configuration interaction method. *J. Chem. Phys.* **1988**, *89*, 5803.

(7) Knowles, P. J.; Werner, H.-J. An efficient method for the evaluation of coupling coefficients in configuration interaction calculations. *Chem. Phys. Lett.* **1988**, *145*, 514.

(8) Köhn, A.; Hanauer, M.; Mück, L. A.; Jagau, T.-C.; Gauss, J. State-specific multireference coupled-cluster theory. *WIREs Comput. Mol. Sci.* **2013**, *3*, 176.

(9) Lyakh, D. I.; Musiał, M.; Lotrich, V. F.; Bartlett, R. J. Multireference Nature of Chemistry: The Coupled-Cluster View. *Chem. Rev.* **2012**, *112*, 182−243.

(10) Kurashige, Y.; Yanai, T. Second-order perturbation theory with a density matrix renormalization group self-consistent field reference function: Theory and application to the study of chromium dimer. *J. Chem. Phys.* **2011**, *135*, 094104.

(11) Jiménez-Hoyos, C. A.; Henderson, T. M.; Tsuchimochi, T.; Scuseria, G. E. Projected Hartree-Fock theory. *J. Chem. Phys.* **2012**, *136*, 164109.

(12) Löwdin, P.-O. Quantum Theory of Many-Particle Systems. III. Extension of the Hartree-Fock Scheme to Include Degenerate Systems and Correlation Effects. *Phys. Rev.* **1955**, *97*, 1509.

(13) Mayer, I.; Ladik, J.; Biczó, G. Spin projected extended Hartree-Fock equations. *Int. J. Quantum Chem.* **1973**, *7*, 583−608.

(14) Mayer, I. The Spin-Projected Extended Hartree-Fock Method. *Adv. Quantum Chem.* **1980**, *12*, 189−262.

(15) Schlegel, H. B. Potential energy curves using unrestricted Møller-Plesset perturbation theory with spin annihilation. *J. Chem. Phys.* **1986**, *84*, 4530.

(16) Schlegel, H. B. Møller-Plesset Perturbation Theory with Spin Projection. *J. Phys. Chem.* **1988**, *92*, 3075−3078.

(17) Knowles, P. J.; Handy, N. C. Convergnce of Projected Unrestricted Hartree-Fock Møller-Plesset Series. *J. Phys. Chem.* **1988**, *92*, 3097−3100.

(18) Knowles, P. J.; Handy, N. C. Projected unrestricted Møller-Plesset second-order energies. *J. Chem. Phys.* **1988**, *88*, 6991.

(19) Tsuchimochi, T.; Van Voorhis, T. Extended Møller-Plesset perturbation theory for dynamical and static correlations. *J. Chem. Phys.* **2014**, *141*, 164117.

(20) Tsuchimochi, T.; Van Voorhis, T. Time-dependent projected Hartree-Fock. *J. Chem. Phys.* **2015**, *142*, 124103.

(21) Tsuchimochi, T.; Ten-no, S. Communication: Configuration interaction combined with spin-projection for strongly correlated molecular electronic structures. *J. Chem. Phys.* **2016**, *144*, 011101.

(22) Tsuchimochi, T.; Ten-no, S. Black-box description of electron correlation with spin-extended configuration interaction model: Implementation and Assessment. *J. Chem. Theory Comput.* **2016**, *12*, 1741−1759.

(23) Duguet, T. Symmetry broken and restored coupled-cluster theory: I. Rotational symmetry and angular momentum. *J. Phys. G: Nucl. Part. Phys.* **2015**, *42*, 025107.

(24) Tsuchimochi, T.; Ten-no, S. Bridging Single- and Multireference Domains for Electron Correlation: Spin-Extended Coupled Electron Pair Approximation. *J. Chem. Theory Comput.* **2017**, *13*, 1667−1681.

(25) Qiu, Y.; Henderson, T. M.; Zhao, J.; Scuseria, G. E. Projected coupled cluster theory. *J. Chem. Phys.* **2017**, *147*, 064111.

(26) Qiu, Y.; Henderson, T. M.; Zhao, J.; Scuseria, G. E. Projected coupled cluster theory: Optimization of cluster amplitudes in the presence of symmetry projection. *J. Chem. Phys.* **2018**, *149*, 164108.

(27) Tsuchimochi, T.; Ten-no, S. L. Orbital-invariant spin-extended approximate coupled-cluster for multi-reference systems. *J. Chem. Phys.* **2018**, *149*, 044109.

(28) Tsuchimochi, T.; Ten-no, S. L. Extending Spin-Symmetry Projected Coupled-Cluster to Large Model Spaces Using an Iterative Null-Space Projection Technique. *J. Comput. Chem.* **2019**, *40*, 265–278.

(29) Sinanoğlu, O. Relation of Perturbation Theory to Variation Method. *J. Chem. Phys.* **1961**, *34*, 1237–1240.

(30) Hylleraas, E. A. Über den Grundterm der Zweielektronenprobleme von H⁻, He, Li⁺, Be⁺² usw. *Eur. Phys. J. A* **1930**, *65*, 209–225.

(31) Celani, P.; Werner, H.-J. Analytical energy gradients for internally contracted second-order multireference perturbation theory. *J. Chem. Phys.* **2003**, *119*, 5044–5057.

(32) Park, J. W.; Al-Saadon, R.; Strand, N. E.; Shiozaki, T. Imaginary Shift in CASPT2 Nuclear Gradient and Derivative Coupling Theory. *J. Chem. Theory Comput.* **2019**, *15*, 4088–4098.

(33) Roos, B. O.; Andersson, K. Multiconfigurational perturbation theory with level shift − the Cr_2 potential revisited. *Chem. Phys. Lett.* **1995**, *245*, 215–223.

(34) Forsberg, N.; Malmqvist, P.-Å. Multiconfiguration perturbation theory with imaginary level shift. *Chem. Phys. Lett.* **1997**, *274*, 196–204.

(35) Ghigo, G.; Roos, B. O.; Malmqvist, P.-Å. A modified definition of the zeroth order hamiltonian in multiconfigurational perturbation theory (CASPT2). *Chem. Phys. Lett.* **2004**, *396*, 142–149.

(36) Malmqvist, P.-Å.; Pierloot, K.; Shahi, A. R. M.; Cramer, C. J.; Gagliardi, L. The restricted active space followed by second-order perturbation theory method: theory and application to the study of CuO_2 and Cu_2O_2 systems. *J. Chem. Phys.* **2008**, *128*, 204109.

(37) Ma, D.; Li Manni, G.; Olsen, J.; Gagliardi, L. Second-Order Perturbation Theory for Generalized Active Space Self-Consistent-Field Wave Functions. *J. Chem. Theory Comput.* **2016**, *12*, 3208–3213.

(38) Kähler, S.; Olsen, J. Non-orthogonal internally contracted multi-configurational perturbation theory (NICPT): Dynamic electron correlation for large, compact active spaces. *J. Chem. Phys.* **2017**, *147*, 174106.

(39) Amos, A. T.; Hall, G. G. Single Determinant Wave Functions. *Proc. R. Soc. London A* **1961**, *263*, 483.

(40) The linear dependence occurs because some of the linear combinations of broken-symmetry singles and doubles do not possess the designated spin component and hence they are null upon the spin projection. Hence, such zeroes appear in the same fashion regardless of the operator.

(41) Jørgensen, P.; Helgaker, T. Møller-Plesset energy derivatives. *J. Chem. Phys.* **1988**, *89*, 1560–1570.

(42) Helgaker, T.; Jørgensen, P. Configuration-interaction energy derivatives in a fully variational formulation. *Theor. Chim. Acta* **1989**, *75*, 111–127.

(43) Lauderdale, W. J.; Stanton, J. F.; Gauss, J.; Watts, J. D.; Bartlett, R. J. Many-body perturbation theory with a restricted open-shell Hartree-Fock reference. *Chem. Phys. Lett.* **1991**, *187*, 21–28.

(44) Gellan, A. *Hierarchical Quantum Chemistry Program*; Kobe University, Kobe, Japan.

(45) Frisch, M. J.; Trucks, G. W.; Schlegel, H. B.; Scuseria, G. E.; Robb, M. A.; Cheeseman, J. R.; Scalmani, G.; Barone, V.; Mennucci, B.; Petersson, G. A.; Nakatsuji, H.; Caricato, M.; Li, X.; Hratchian, H. P.; Izmaylov, A. F.; Bloino, J.; Zheng, G.; Sonnenberg, J. L.; Hada, M.; Ehara, M.; Toyota, K.; Fukuda, R.; Hasegawa, J.; Ishida, M.; Nakajima, T.; Honda, Y.; Kitao, O.; Nakai, H.; Vreven, T.; Montgomery, J. A., Jr.; Peralta, J. E.; Ogliaro, F.; Bearpark, M.; Heyd, J. J.; Brothers, E.; Kudin, K. N.; Staroverov, V. N.; Kobayashi, R.; Normand, J.; Raghavachari, K.; Rendell, A.; Burant, J. C.; Iyengar, S. S.; Tomasi, J.; Cossi, M.; Rega, N.; Millam, J. M.; Klene, M.; Knox, J. E.; Cross, J. B.; Bakken, V.; Adamo, C.; Jaramillo, J.; Gomperts, R.; Stratmann, R. E.; Yazyev, O.; Austin, A. J.; Cammi, R.; Pomelli, C.; Ochterski, J. W.; Martin, R. L.; Morokuma, K.; Zakrzewski, V. G.; Voth, G. A.; Salvador, P.; Dannenberg, J. J.; Dapprich, S.; Daniels, A. D.; Foresman, J. B.; Ortiz, J. V.; Cioslowski, J.; Fox, D. J. *Gaussian 09*, Revision D.01; Gaussian Inc.: Wallingford, CT, 2009.

(46) Werner, H.-J.; Knowles, P. J.; Knizia, G.; Manby, F. R.; Schütz, M. Molpro: a general - purpose quantum chemistry program package. *WIREs Comput. Mol. Sci.* **2012**, *2*, 242–253.

(47) Tsuchimochi, T.; Scuseria, G. E. ROHF theory made simple. *J. Chem. Phys.* **2010**, *133*, 141102.

(48) Tsuchimochi, T.; Scuseria, G. E. Constrained active space unrestricted mean-field methods for controlling spin-contamination. *J. Chem. Phys.* **2011**, *134*, 064101.

(49) Pulay, P. Convergence acceleration of iterative sequences. the case of SCF iteration. *Chem. Phys. Lett.* **1980**, *73*, 393–398.

(50) Pulay, P. Improved SCF convergence acceleration. *J. Comput. Chem.* **1982**, *3*, 556–560.

(51) Hehre, W. J.; Ditchfield, R.; Pople, J. A. Self-Consistent Molecular Orbital Methods. XII. Further Extensions of Gaussian-Type Basis Sets for Use in Molecular Orbital Studies of Organic Molecules. *J. Chem. Phys.* **1972**, *56*, 2257.

(52) We should, however, note that this is only a rough estimate because we treat real and imaginary level shifts in a slightly different manner. See above.

(53) Krogh, J. W.; Olsen, J. A general coupled cluster study of the N_2 molecule. *Chem. Phys. Lett.* **2001**, *344*, 578–586.

(54) Yanai, T.; Chan, G. K.-L. Canonical transformation theory for multireference problems. *J. Chem. Phys.* **2006**, *124*, 194106.

(55) Hanauer, M.; Köhn, A. Pilot applications of internally contracted multireference coupled cluster theory, and how to choose the cluster operator properly. *J. Chem. Phys.* **2011**, *134*, 204111.

(56) Manni, G. L.; Carlson, R. K.; Luo, S.; Ma, D.; Olsen, J.; Truhlar, D. G.; Gagliardi, L. Multiconfiguration Pair-Density Functional Theory. *J. Chem. Theory Comput.* **2014**, *10*, 3669.

(57) Kendall, R. A.; Dunning, T. H.; Harrison, R. J. Electron affinities of the first-row atoms revisited. Systematic basis sets and wave functions. *J. Chem. Phys.* **1992**, *96*, 6796–6806.

(58) Huber, K. P.; Herzberg, G. *Constants of Diatomic Molecules*; Van Nostrand Reinhold: New York, 1979.

(59) Purvis, G. D.; Bartlett, R. J. A full coupled-cluster singles and doubles model: The inclusion of disconnected triples. *J. Chem. Phys.* **1982**, *76*, 1910–1918.

(60) Jiménez-Hoyos, C. A.; Rodríguez-Guzmán, R.; Scuseria, G. E. Excited electronic states from a variational approach based on symmetry-projected Hartree-Fock configurations. *J. Chem. Phys.* **2013**, *139*, 224110.

(61) Rivero, P.; Jiménez-Hoyos, C. A.; Scuseria, G. E. Predicting Singlet-Triplet Energy Splittings with Projected Hartree-Fock Methods. *J. Phys. Chem. A* **2013**, *117*, 8073–8080.

(62) Slipchenko, L. V.; Krylov, A. I. Singlet-triplet gaps in diradicals by the spin-flip approach: A benchmark study. *J. Chem. Phys.* **2002**, *117*, 4694.

(63) Pulay, P.; Hamilton, T. P. UHF natural orbitals for defining and starting MC-SCF calculations. *J. Chem. Phys.* **1988**, *88*, 4926–4933.

(64) Bofill, J. M.; Pulay, P. The unrestricted natural orbital-complete active space (UNO-CAS) method: An inexpensive alternative to the complete active space-self-consistent-field (CAS-SCF) method. *J. Chem. Phys.* **1989**, *90*, 3637–3646.

(65) Jensen, H. J. A.; Jørgensen, P.; Ågren, H.; Olsen, J. Second-order Møller-Plesset perturbation theory as a configuration and orbital generator in multiconfiguration self-consistent field calculations. *J. Chem. Phys.* **1988**, *88*, 3834–3839.

(66) Abrams, M. L.; Sherrill, C. D. Natural orbitals as substitutes for optimized orbitals in complete active space wavefunctions. *Chem. Phys. Lett.* **2004**, *395*, 227–232.

(67) Stein, C. J.; Reiher, M. Automated Selection of Active Orbital Spaces. *J. Chem. Theory Comput.* **2016**, *12*, 1760–1771.

(68) Sayfutyarova, E. R.; Sun, Q.; Chan, G. K.-L.; Knizia, G. Automated Construction of Molecular Active Spaces from Atomic Valence Orbitals. *J. Chem. Theory Comput.* **2017**, *13*, 4063−4078.

(69) Armstrong, A. T.; Smith, F.; Elder, E.; McGlynn, S. P. Electronic Absorption Spectrum of Ferrocene. *J. Chem. Phys.* **1967**, *46*, 4321−4328.

(70) Lin, C.-H.; Pursley, D.; Klein, J. E. M. N.; Teske, J.; Allen, J. A.; Rami, F.; Köhn, A.; Plietker, B. Non-decarbonylative photochemical versus thermal activation of $Bu_4N[Fe(CO)_3(NO)]^-$ the Fe-catalyzed Cloke-Wilson rearrangement of vinyl and arylcyclopropanes. *Chem. Sci.* **2015**, *6*, 7034−7043.

(71) Angeli, C.; Cimiraglia, R.; Evangelisti, S.; Leininger, T.; Malrieu, J.-P. Introduction of n-electron valence states for multi-reference perturbation theory. *J. Chem. Phys.* **2001**, *114*, 10252−10264.

(72) Angeli, C.; Cimiraglia, R.; Malrieu, J.-P. N-electron valence state perturbation theory: a fast implementation of the strongly contracted variant. *Chem. Phys. Lett.* **2001**, *350*, 297−305.

(73) Angeli, C.; Cimiraglia, R.; Malrieu, J.-P. n-electron valence state perturbation theory: A spinless formulation and an efficient implementation of the strongly contracted and of the partially contracted variants. *J. Chem. Phys.* **2002**, *117*, 9138−9153.

(74) Harding, M. E.; Metzroth, T.; Gauss, J.; Auer, A. A. Parallel Calculation of CCSD and CCSD(T) Analytic First and Second Derivatives. *J. Chem. Theory Comput.* **2008**, *4*, 64−74.

(75) Ishimura, K.; Hada, M.; Nakatsuji, H. Ionized and excited states of ferrocene: Symmetry adapted cluster-configuration-interaction study. *J. Chem. Phys.* **2002**, *117*, 6533−6537.

(76) Klein, J. E. M. N.; Miehlich, B.; Holzwarth, M. S.; Bauer, M.; Milek, M.; Khusniyarov, M. M.; Knizia, G.; Werner, H.-J.; Plietker, B. The Electronic Ground State of $[Fe(CO)_3(NO)]^-$: A Spectroscopic and Theoretical Study. *Angew. Chem., Int. Ed.* **2014**, *53*, 1790−1794.

(77) Andersson, K.; Roos, B. O.; Malmqvist, P.-Å.; Widmark, P.-O. The Cr_2 potential energy curve studied with multiconfigurational second-order perturbation theory. *Chem. Phys. Lett.* **1994**, *230*, 391−397.

(78) Stoll, H. The Cr_2 potential curve: a multireference pair functional treatment. *Mol. Phys.* **1996**, *88*, 793−802.

(79) Dachsel, H.; Harrison, R. J.; Dixon, D. A. Multireference Configuration Interaction Calculations on Cr_2: Passing the One Billion Limit in MRCI/MRACPF Calculations. *J. Phys. Chem. A* **1999**, *103*, 152−155.

(80) Müller, T. Large-Scale Parallel Uncontracted Multireference-Averaged Quadratic Coupled Cluster: The Ground State of the Chromium Dimer Revisited. *J. Phys. Chem. A* **2009**, *113*, 12729−12740.

(81) Coe, J.; Murphy, P.; Paterson, M. Applying Monte Carlo configuration interaction to transition metal dimers: Exploring the balance between static and dynamic correlation. *Chem. Phys. Lett.* **2014**, *604*, 46−52.

(82) Purwanto, W.; Zhang, S.; Krakauer, H. An auxiliary-field quantum Monte Carlo study of the chromium dimer. *J. Chem. Phys.* **2015**, *142*, 064302.

(83) Vancoillie, S.; Malmqvist, P.-Å.; Veryazov, V. Potential Energy Surface of the Chromium Dimer Re-re-revisited with Multiconfigurational Perturbation Theory. *J. Chem. Theory Comput.* **2016**, *12*, 1647−1655.

(84) Guo, S.; Watson, M. A.; Hu, W.; Sun, Q.; Chan, G. K.-L. N-Electron Valence State Perturbation Theory Based on a Density Matrix Renormalization Group Reference Function, with Applications to the Chromium Dimer and a Trimer Model of Poly(p-Phenylenevinylene) Sheng. *J. Chem. Theory Comput.* **2016**, *12*, 1583−1591.

(85) Sokolov, A. Y.; Chan, G. K.-L. A time-dependent formulation of multi-reference perturbation theory. *J. Chem. Phys.* **2016**, *144*, 064102.

(86) Casey, S. M.; Leopold, D. G. Negative ion photoelectron spectroscopy of chromium dimer. *J. Phys. Chem.* **1993**, *97*, 816−830.

(87) Su, C.-X.; Hales, D. A.; Armentrout, P. The bond energies of Cr_2 and cr_2^+. *Chem. Phys. Lett.* **1993**, *201*, 199−204.

(88) Hilpert, K.; Ruthardt, R. Determination of the Dissociation Energy of the Cr_2 Molecule. *Ber. Bunsenges. Phys. Chem.* **1987**, *91*, 724.

(89) Simard, B.; Lebeault-Dorget, M.-A.; Marijnissen, A.; ter Meulen, J. J. Photoionization spectroscopy of dichromium and dimolybdenum: Ionization potentials and bond energies. *J. Chem. Phys.* **1998**, *108*, 9668.

(90) Tsuchimochi, T.; Ten-no, S. General technique for analytical derivatives of post-projected Hartree-Fock. *J. Chem. Phys.* **2017**, *146*, 074104.

(91) Head-Gordon, M.; Rico, R. J.; Oumi, M.; Lee, T. J. A doubles correction to electronic excited states from configuration interaction in the space of single substitutions. *Chem. Phys. Lett.* **1994**, *219*, 21−29.